Metallurgical and Thermal Processing Investigation of Additively Manufactured Superalloys JBK-75 and NASA-HR-1

A Senior Project
Presented to the Faculty of the Materials Engineering Department
California Polytechnic State University, San Luis Obispo

In Partial Fulfillment
Of the Requirements for the Degree
Bachelor of Science, Materials Engineering

By
Allyse Birken, Derek Noel
Advisor: Prof. Blair London
Sponsor: Aerojet Rocketdyne
June 2021

Abstract

Aerojet Rocketdyne is investigating the use of directed energy deposition (DED), an additive manufacturing process, to reduce cost and lead time for manufacturing complex rocket engine components for their RS-25 engines. JBK-75 and NASA-HR-1, two Fe-Ni-base, age-hardenable (γ') superalloys, are used for nozzle structural jackets and hot gas manifolds. Currently, these parts are produced using traditional forging or casting methods followed by intensive machining operations. Additionally, these alloys were designed for use in the wrought condition and require a different set of post-processing heat treatments when produced using DED due to their dendritic, segregated microstructure in the as-built condition. Homogenization heat treatment is necessary to transform the dendritic structure into an equiaxed, homogenous structure prior to aging to achieve optimum properties. The team characterized a set of homogenization heat treatments with varying parameters to better understand how homogenization affects the alloys' room temperature mechanical properties and microstructure. Characterization techniques used include metallography and tensile testing at room temperature. The heat treated JBK-75 DED samples all met or were close to the yield strength of wrought, heat treated JBK-75. Homogenization heat treatment time and temperature did not have a significant effect on the yield or tensile strength of JBK-75. The NASA-HR-1 DED samples were sensitive to artifacts of the DED process such as porosity and surface finish, as samples with high porosity and poor surface finish displayed poor ductility. All NASA-HR-1 samples exhibited poor strength and did not meet the strength of the wrought material. All homogenization heat treatments were successful in producing a homogeneous, equiaxed microstructure, but considerable grain growth occurred, which caused lower strengths for both alloys.

Keywords

Superalloy, Fe-Ni-base, JBK-75, NASA-HR-1, additive manufacturing, directed energy deposition, homogenization, heat treatment, metallography, tensile testing, rocket engine, materials engineering

Acknowledgements

We would like to thank Bryce Simmons, Matthew Williams, Greg Kayser (Aerojet Rocketdyne) and Paul Gradl (NASA) for sponsoring this project. Additionally, thank you to Dr. Blair London (California Polytechnic State University – San Luis Obispo, Materials Engineering) for providing guidance as our project advisor. Thank you to Eric Beaton (California Polytechnic State University – San Luis Obispo, Materials Engineering) and the Materials Engineering department. Finally, thank you to Louis Gerny, Aditya Garg, and Bryan Neill (California Polytechnic State University – San Luis Obispo, Machine Shops) for machining sample specimens.

Contents

List of Figures

List of Tables

1. Introduction

1.1 Sponsor Information

Aerojet Rocketdyne is the premier propulsion system supplier for the space and defense industry. Notable rocket engines produced by Aerojet Rocketdyne include the RS-25 and RL10 liquid bipropellant engines. These reusable engines utilize liquid hydrogen fuel and a liquid oxygen oxidizer to produce 418,000 pounds of thrust in the main combustion chamber (MCC) [1]. The RS-25 engine (Figure 1) is more commonly known for being the main engine used on the space shuttle. This engine helped power the Space Shuttle through 135 missions.

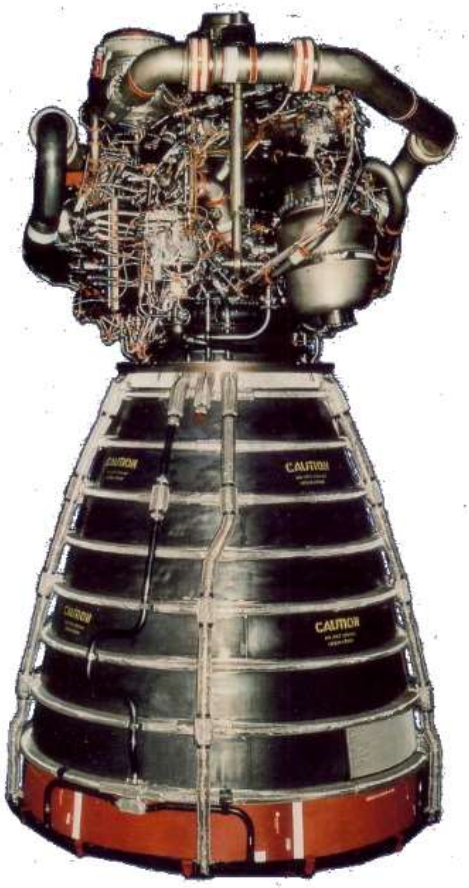

Figure 1. RS-25 liquid bipropellant engine built by Aerojet Rocketdyne. The diameter of the nozzle is 90″, making it a strong candidate for large scale additive manufacturing [2].

A new generation of these engines is currently contracted to be used on NASA's Space Launch System (SLS), as seen in Figure 2. A group of four of these engines will be used to power their heavy launch vehicles with more than 2 million pounds of thrust [1].

Figure 2. Four RS-25 engines secured into the SLS launch vehicle [3].

1.2 Application and End-Use

Aerojet Rocketdyne is investigating the use of additive manufacturing to produce rocket engine components for the RS-25 and other rocket engines. Currently, they manufacture these rocket engine components using traditional manufacturing processes like forging and casting.

A rocket engine utilizes a series of components, like valves and pumps, to produce thrust (Figure 3). First, liquid hydrogen fuel and liquid oxygen oxidizer flow through independent lines into the Main Propulsion System (MPS) from the rockets' core. The fuel and oxidizer are then sent to the each of the engines on the launch vehicle. Then, valves on each engine open to allow the fuel and oxidizer into the engine. Inside the engine, the fuel and oxidizer will then flow through the low-pressure oxidizer and fuel turbopumps (LPOTP and LPFTP) and high pressure turbopumps (HPOTP and HPFTP). The fuel and oxidizer are then separated and flow through different channels. The fuel will flow to the regenerative cooling system to cool the nozzle and main combustion chamber (MCC). It then passes through injectors where it will be mixed with the oxidizer and ignited in the MCC [4].

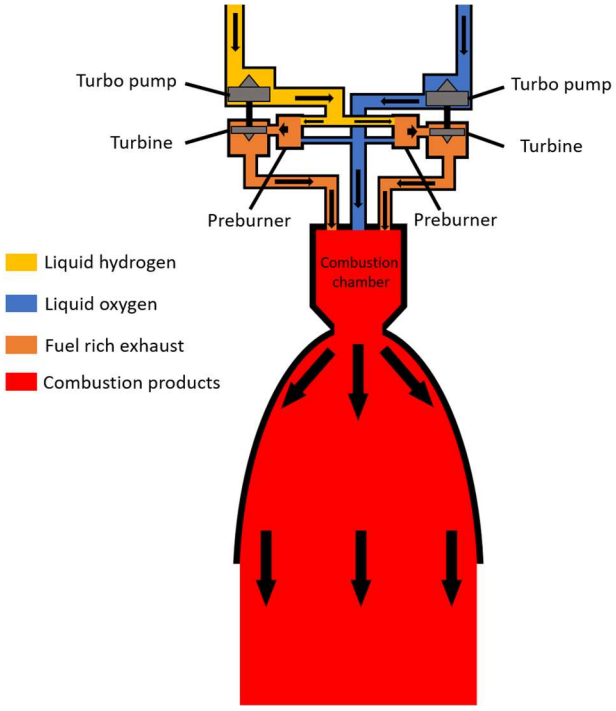

Figure 3. Simplified process schematic of the RS-25 engine system [5].

Several examples of rocket engine components being investigated for production via additive manufacturing include nozzle and main combustion chamber jackets and manifolds. Figure 4a shows a schematic of a rocket nozzle that has a separated nozzle liner and nozzle jacket. The separate nozzle liner and jacket are typically bonded together at the vertical ribs of the liner, producing cooling internal channels. During use, these channels circulate coolant to keep the nozzle temperature low [6]. Brazing is a typical method for producing this joint, but other methods can also be used.

Additive manufacturing can also be used to produce monolithic nozzles with integrated cooling channels, as shown in Figure 4b. Producing these monolithic nozzles with integrated cooling channels removes the need for the complex joining process for bonding the liner to the jacket [6]. Using additive manufacturing to produce these components has the potential to drastically reduce cost and lead time for these parts – these parts traditionally require intensive machining processes, but the complex geometry possible with additive manufacturing has the potential to reduce the amount of machining operations needed, which reduces cost and lead time. Currently, Aerojet Rocketdyne and NASA are investigating directed energy deposition (DED) and selective laser melting (SLM) processes for this hardware.

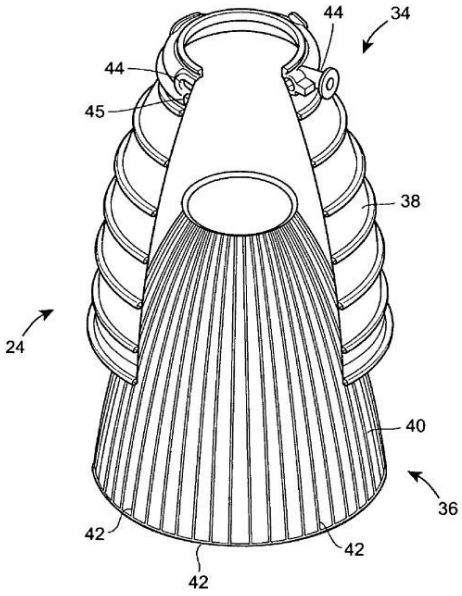

a.

b.

Figure 4a. Rocket nozzle schematic with separated liner and jacket. The jacket is the top component, and the liner is the vertically ribbed bottom component [7]. Figure 4b. Rocket nozzle with integrated cooling channels [6].

This application presents challenging material property requirements. The nozzle jacket material must have a high yield strength at high temperatures to support stresses from the internal pressure from hot gases coming out of the main combustion chamber (Figure 5). The nozzle jacket material must also have a high enough thermal conductivity such that it can easily transfer heat to the coolant in the nozzle. Furthermore, the material must have sufficient ductility – it is better for these parts to yield during use than to crack. Lastly, since hydrogen gases are involved in the combustion reaction, the material must be resistant to hydrogen embrittlement [8].

Figure 5. NASA hot fire testing of prototype DED rocket nozzle jacket [6].

A-286 and JBK-75, two Fe-Ni-base superalloys, meet these material property criteria and are commonly used for these parts. They possess good strength at the necessary operating temperatures in addition to having adequate resistance to both hydrogen embrittlement and corrosion. NASA also developed an alloy that was derived from JBK-75, called NASA-HR-1,

that has higher strength and higher resistance to hydrogen embrittlement [8]. Additionally, JBK-75 and NASA-HR-1 have better weldability than A-286, making them prime candidates for additive manufacturing [9].

1.3 JBK-75 and NASA-HR-1 Superalloys

JBK-75 and NASA-HR-1 are fully austenitic, precipitation-hardening iron-nickel-base superalloys. These alloys have a combination of high temperature yield strength, corrosion/oxidation resistance, and resistance to hydrogen embrittlement [8].

In iron-nickel-base superalloys, the FCC austenite phase (γ) is the matrix phase, and this phase is stable from room temperature up to high temperatures. Since the matrix is austenitic, precipitation reactions occur at high temperatures. This results in strong alloys that can be used at higher service temperatures without the risk of overaging [10]. As shown in Figure 6, NASA-HR-1 does not experience a significant strength drop until 1200°F due to its γ′ precipitates that are stable up to those high temperatures [11]. Additionally, the FCC matrix is much tougher than its BCC counterpart, such as in the martensitic and semi-austenitic precipitation-hardening stainless steels.

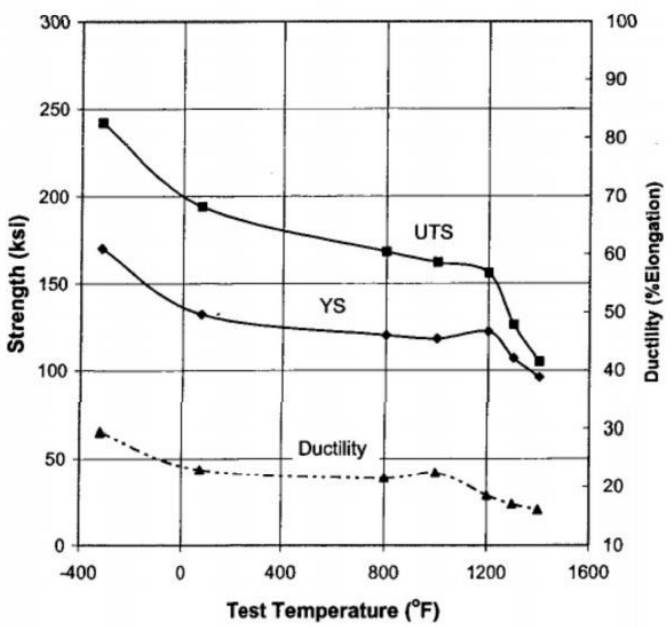

Figure 6. NASA HR-1 strength and ductility as a function of temperature. Notice that the alloy does not experience a precipitous strength drop until 1200°F [11].

The nominal compositions of the alloys are shown in Table I. JBK-75 was originally developed based on A-286, a commercial precipitation-hardening stainless steel. JBK-75 has small composition changes, such as tighter limits for the manganese and silicon content that mainly improve weldability, as well as an increased nickel content. These chemistry changes also improve JBK-75's ability to be additively manufactured, since welding and additive manufacturing processes both feature high, localized heating and cooling rates [9].

In all three alloys, the austenite phase is stable at room temperature. This is attributed to the high nickel content, as nickel is a strong austenite stabilizer and decreases the martensite start temperature – high enough austenite stabilization pushes the martensite start temperature to sub-zero temperatures, meaning the austenite phase is stable to room temperature even on quenching from high temperature [10].

As mentioned earlier, these fully austenitic alloys are age-hardenable. Small titanium and aluminum additions (shown in Table I) allow for precipitation of the $Ni_3(Ti, Al)$ intermetallic phase, γ', which is coherent with the FCC matrix [12].

Lastly, the alloys' high corrosion and oxidation resistance can be attributed to the alloy's chromium and aluminum contents. At lower temperatures, Cr_2O_3 forms and protects against oxidation and corrosion. At higher temperatures, the Cr_2O_3 film breaks down and Al_2O_3 forms, still protecting the metal from oxidation [12].

Table I. Nominal Compositions of JBK-75 and NASA-HR-1 with Alloying Element Functions [8, 12]

Content (wt%)	A-286	JBK-75	NASA-HR-1	Alloying Element Function
Fe	Bal.	Bal.	Bal.	Primary alloy constituent, phase stability
Ni	25.5	30	35	Austenite stabilizer
Ti	2.1	2.2	2.5	γ' former (Ni_3Ti, Al)
Al	0.2	0.3	0.3	γ' former (Ni_3Ti, Al)
Cr	14.8	14.8	15	Corrosion resistance, solid solution strengthening
Mo	1.3	1.3	2	Reduces solidification cracking susceptibility
Co	-	-	3.3	Austenite phase stability
W	-	-	1.8	Solid solution strengthening, slows grain boundary η formation
V	0.3	0.3	0.3	Improved notch toughness
C	0.015 max.	0.015 max.	0.01 max.	Forms carbides with Ti, V, Cr, Mo

These alloys are typically used in the solution treated and aged (STA) condition. The standard solution treat and age used by Aerojet Rocketdyne is solution treating at 1800°F for 1 hour, oil quench, and age at 1375°F for 16 hours. These aging treatments must be long due to the slow diffusion of titanium. Figure 7 shows the time-temperature-precipitation (TTP) diagram for A-286 and JBK-75 [13]. Notice that the aging temperature of 1375°F is in the γ' regime, but low enough to avoid substantial precipitation of the η phase. The η phase is an incoherent form of Ni_3Ti that forms at the grain boundaries with an acicular or cellular morphology [11]. Substantial presence of this phase is detrimental to ductility and typically forms during overaging or prolonged high temperature exposure. Some amount of (Ti, Mo)C carbide precipitation also occurs during the standard aging heat treatment.

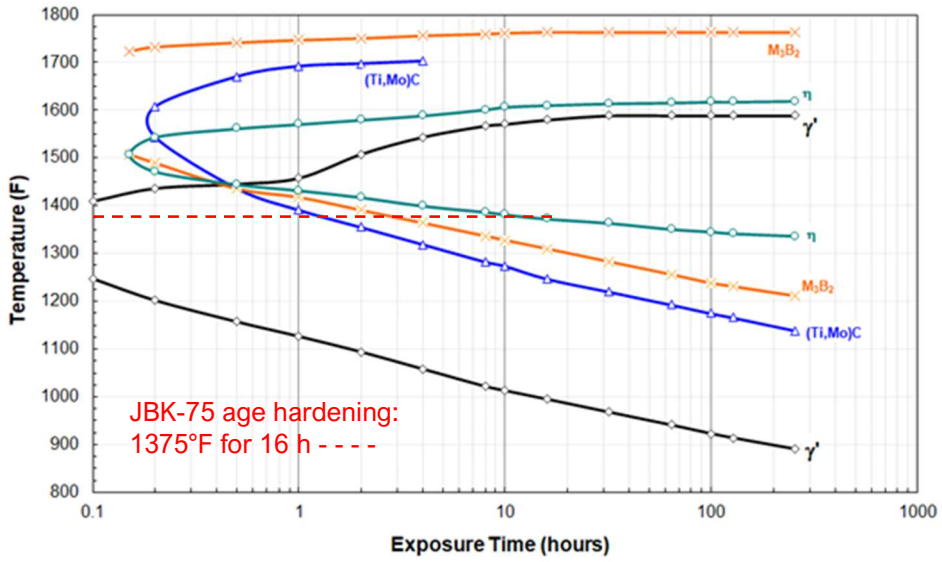

Figure 7. Time-temperature-precipitation diagram for start of precipitation reactions in solution treated JBK-75. The standard aging treatment has been labeled as the dashed line on the plot [13].

A typical microstructure for A-286 in the STA condition is shown in Figure 8a. Notice that γ is the only phase visible at this magnification, and all γ′ precipitates are only visible at higher magnifications, yet these precipitates are responsible for the high strength of this alloy.

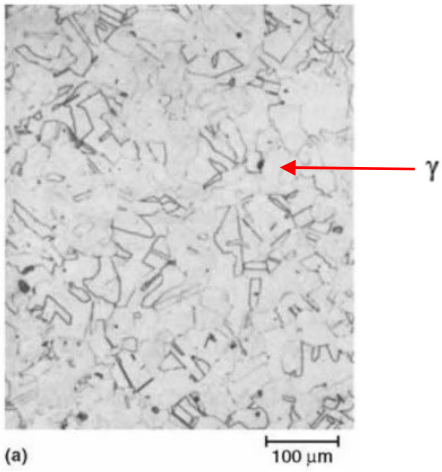

Figure 8. Microstructure of wrought A-286 in the STA condition. Etched, 400X magnification [10].

The STA heat treatment results in a substantial increase in strength for these alloys. Table II shows the mechanical properties of A-286 in both the solution treated condition and the solution treated and aged condition. Notice that a high level of ductility is retained in the material even at the peak aged condition – this can be attributed to the alloy's FCC crystal structure and its high number of slip systems.

Table II. Effects of Aging on Room Temperature Yield Strength and Ductility of A-286 [12]

Condition	Yield strength (ksi)	% Elongation
Solution treated	35	52
Solution treated + aged	104	25

Table III shows a summary of mechanical properties for A-286, JBK-75, and NASA-HR-1 in the STA condition. Notice that NASA-HR-1 has a substantially higher strength than both A-286 and JBK-75, showing the effects of the increased alloying additions in NASA-HR-1.

Table III. Mechanical Properties of A-286, JBK-75, and HR-1 in the STA Condition [11]

Alloy	Yield strength (ksi)	Tensile strength (ksi)	% Elongation
A-286	104	157	25
JBK-75	108	164	27
NASA-HR-1	137	183	24

1.4 Additive Manufacturing Processes

Commonly known as 3D printing, additive manufacturing is a manufacturing process that constructs a part through the addition of material from a solid, digital model. Additive manufacturing is a completely computer-controlled process – from the material deposition to the model data translation. Layer upon layer, additive manufacturing allows for the economic fabrication of parts with complex geometries and features. There are seven main categories of AM commercially available for product production: Sheet Lamination (SHL), Material Jetting (MJT), Binder Jetting (BJT), Vat Photopolymerization (VPP), Powder Bed Fusion (PBF), Material Extrusion (MEX), and Direct Energy Deposition (DED) [15]. This project will focus on DED.

DED is an additive manufacturing process that specializes in making parts of large volume (greater than 1000 mm^3) in addition to having the ability to repair features on preexisting parts [10]. This process features a focused energy beam (laser, plasma, or electron beam) in contact with a material. Material, delivered through a feedstock, is usually found in the metal wire or powder form. The feedstock pushes the material through the feed nozzle, where it then meets the energy beam. The energy beam-material contact causes the material to melt and deposit on to the build platform or piece printing (Figure 9). DED is commonly performed in a sealed chamber of inert gas to prevent oxidation from occurring on the material as well as to improve the control of the printed material properties.

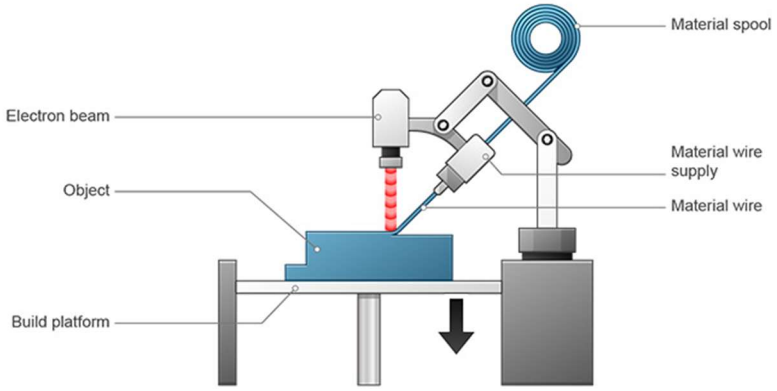

Figure 9. Labeled schematic of directed energy deposition with wire formed material [16].

As with other as-built components, the microstructures seen within DED manufactured components vary depending on the build direction. The orientation in which the sample is cut relative to the build direction will alter the observed morphology of the microstructure. Typically, a sample cut transverse to the build direction, long, columnar dendritic grains are observed, as seen in Figure 10. The dendrites grow in direction of melt pool solidification. Thus, their cores would be observed in the microstructure normal to the build direction.

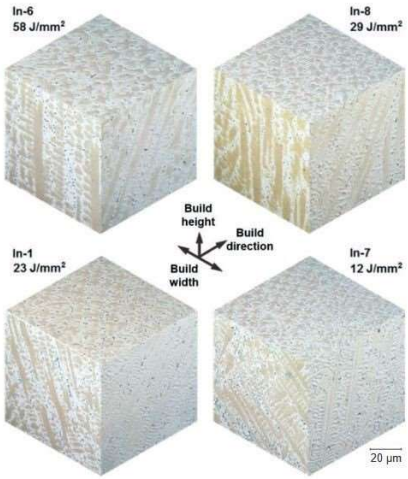

Figure 10. Four micrographs of DED-manufactured Inconel 625. Each micrograph cube was build using a laser with different energy densities. The microstructures shown on each face of the cube display the different morphologies observed depending on the build direct. [17]

The technology behind directed energy deposition presents many benefits. DED is capable of fabricating large metal components at higher speeds than other additive processes. In DED processing, unfused powder can be reused [18]. Thus, DED ultimately produces little to no waste material, which makes it more efficient and cost friendly. However, DED will produce a part with low resolution. This leads to a poor surface finish, which then must be post-machined [16]. This post-machining is expensive and time-consuming. Additionally, support structures are not

viable when using DED. Without support structures for a part, the geometry can be limited and needs to be carefully designed.

1.5 Problem Statement

Aerojet Rocketdyne is investigating the use of additive manufacturing (AM) to produce parts for the RS-25 rocket engine. Using additive manufacturing to produce these complex parts presents a possibility for dramatic cost and lead time reductions. JBK-75 and NASA-HR-1, two age-hardenable (γ'), Fe-Ni-base superalloys, are commonly used for these rocket engine components – these alloys are used in structural jackets and manifolds for both nozzles and main combustion chambers. Currently, these parts are produced using traditional casting or forging methods followed by intensive machining operations. Aerojet Rocketdyne is interested in using directed energy deposition (DED), an AM process, to produce these parts. However, these alloys were designed for use in the wrought condition and require a different set of post-processing heat treatments when produced using DED due to their dendritic, segregated microstructure in the as-built condition compared to a typical wrought, equiaxed structure. Homogenization heat treatment is typically used to remove the microsegregation in the microstructure and to transform the microstructure from dendritic to homogeneous and equiaxed. For JBK-75 and NASA-HR-1, these post-processing heat treatments have not been fully developed. Therefore, the senior project team's goal is to characterize the effect of varying post-processing heat treatments, specifically homogenization, on these alloys' room temperature mechanical properties and microstructure in the age hardened condition. Metallographic examination will be used to evaluate the effect of heat treatment on microstructure, and room temperature tensile testing will be used to assess the effects of heat treatment on mechanical properties in the STA condition.

2. Experimental Procedure

2.1 Heat Treatment Experimental Design

The design of experiment for the heat treatment of both JBK-75 and NASA-HR-1 samples focused on the effects of the homogenization heat treatment on final properties in the STA condition. Two homogenization temperatures were selected and paired with three different times. The two temperatures selected were 2000°F and 2200°F and the times selected were 2, 8, and 16 hours. JBK-75 homogenization temperatures were selected using a time-temperature-precipitation curve (Figure 11).

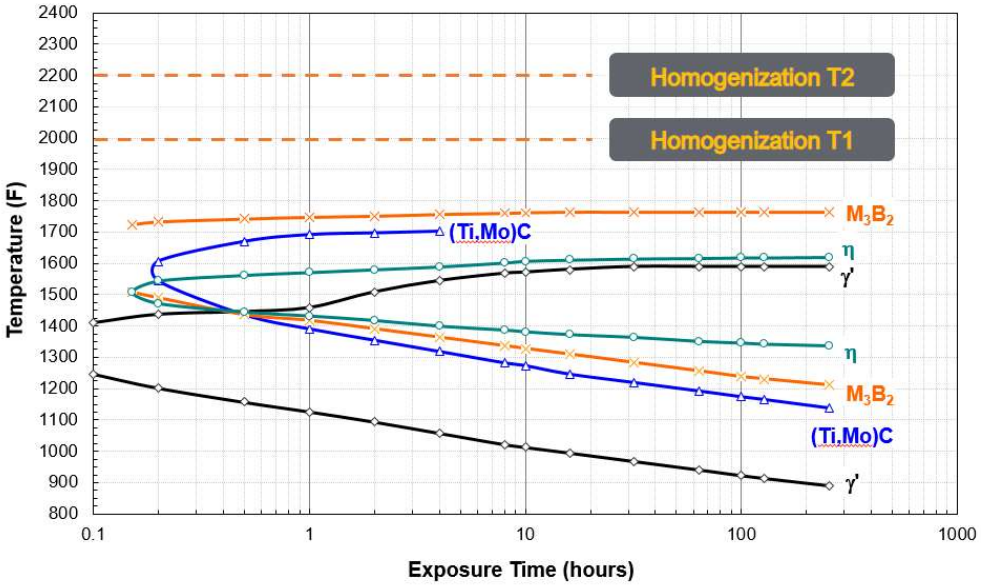

Figure 11. JBK-75 time-temperature-precipitation diagram provided by Aerojet Rocketdyne [13].

The TTP diagram shows that at higher temperatures, the homogenization heat treatment would allow for solid state diffusion of the segregated alloying elements while being above the solvus temperature for any secondary phases. The homogenization heat treatments, after holding for the specified time, were followed by a quench. The purpose of quenching is to prevent slow cooling through the different precipitation regimes of deleterious secondary phases. Following homogenization, all the JBK-75 samples were put through a given, standard solution treat and age heat treatment. The JBK-75 samples did not go through a stress relief heat treatment as they were received already detached from the build plate (Figure 12). All heat treatments were done at Aerojet Rocketdyne in vacuum to prevent substantial oxidation. The homogenization temperatures and times were the same for NASA-HR-1 as per recommendation from given NASA resources (Figure 13). The STA heat treatments for NASA-HR-1 were also given by NASA.

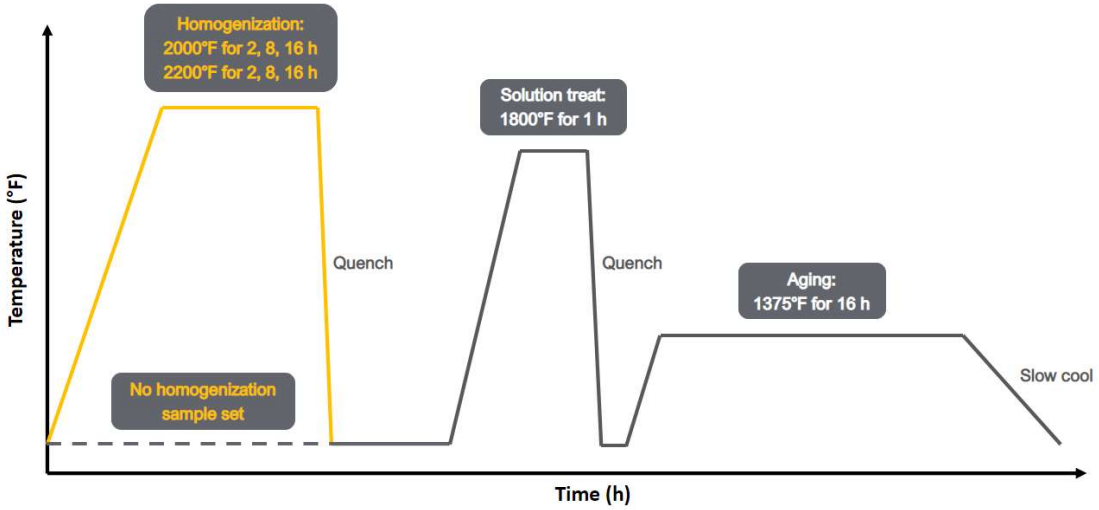

Figure 12. Heat treatment profile for JBK-75 samples. Each sample had unique time/temp combinations for the homogenization step. The solution treating and aging treatments were held consistent throughout the study.

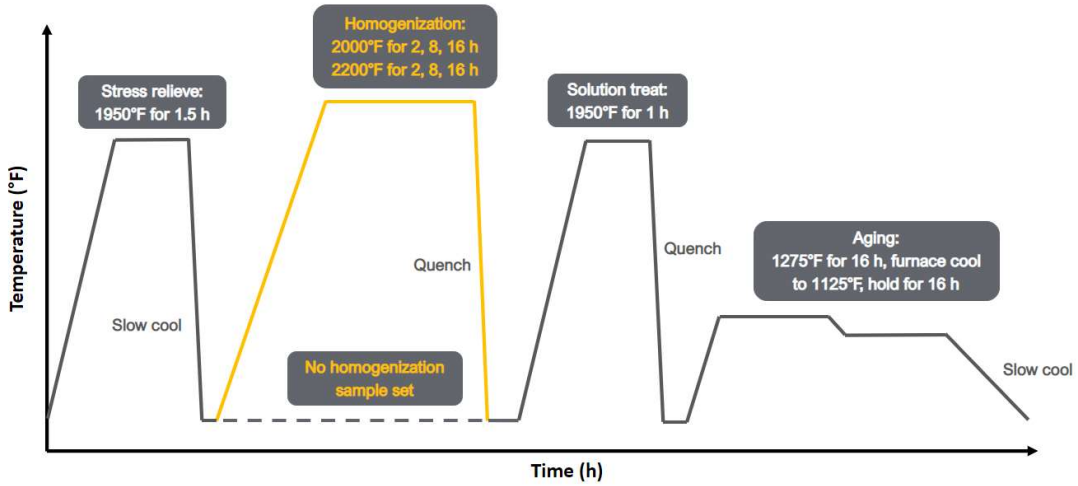

Figure 13. Heat treatment profile for NASA-HR-1 samples. This heat treatment profile is consistent to JBK-75. However, a stress relief heat treatment was done on this alloy as the as-deposited samples were received attached to the build plate.

However, the NASA-HR-1 samples were submitted to a stress relief heat treatment. This was done since these samples were received attached to the build plate. The stress relief heat treatment on the NASA-HR-1 was done in-house at California Polytechnic State University – San Luis Obispo. All NASA-HR-1 samples were placed into stainless steel bags to prevent oxidation from occurring on the sample (Figure 14).

Figure 14. Stainless steel bag used to protect the NASA-HR-1 samples from oxidizing in the heat treatment furnace.

Following the stress relief and homogenization heat treatments, all the samples went through standard solution treat and aging heat treatments standardized by Aerojet Rocketdyne. The rest of the NASA-HR-1 heat treatments were done by Aerojet Rocketdyne.

2.2 Sample Preparation

Three as-deposited JBK-75 samples, provided by Aerojet Rocketdyne, were received in the form of rectangular blocks (Figure 15a). Each sample block was waterjet cut into bars and separated for as-built characterization and heat treatment (Figure 15b).

a. b.

Figure 15. As deposited JBK-75 before and after waterjet cutting. A total of 29 bars were cut from the three as-deposited samples.

After the JBK-75 bars were heat treated, they were CNC machined into tensile specimens following the ASTM E8 subsize specimen dimensions as shown in Figure 16 [19].

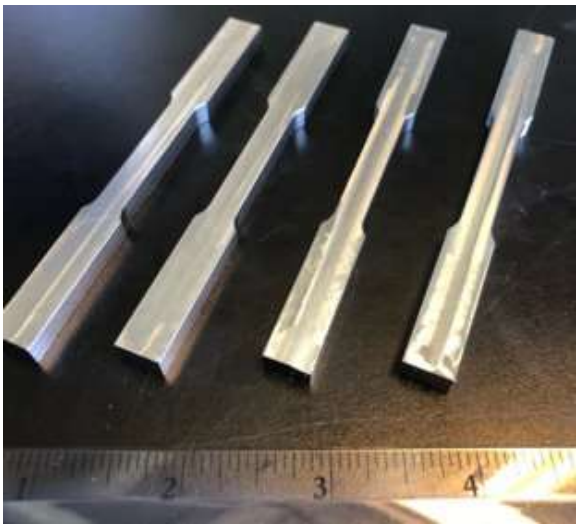

Figure 16. CNC machined JBK-75 tensile bars.

As-deposited NASA-HR-1 material, provided by NASA, was received in the form of two thin-walled boxes attached to the build plate. The two samples received were produced with different (proprietary) processing parameters from two different suppliers and were treated independently throughout the project. Throughout the following sections, the dark-colored box will be referred to as Box 1 NASA-HR-1, while the light-colored box will be referred to as Box 2 NASA-HR-1 (Figure 17a). Panels were cut off each box and then stress relieved. Tensile specimens were waterjet into the post stress relieved panel faces (Figure 17b). The tensile bars were sized based off ASTM E8 subsize specimen dimension.

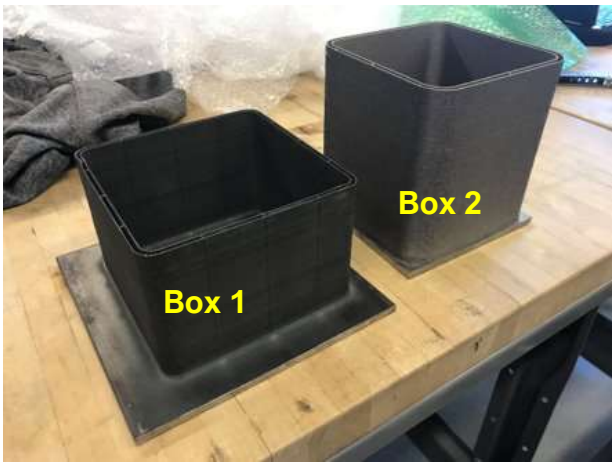

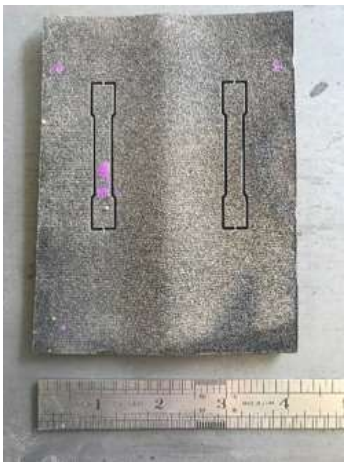

Figure 17a. As-deposited NASA-HR-1 boxes. Figure 17b. Panel cut out of Box 2 with tensile specimens cut out. A total of 24 tensile specimens were machined. The extras from the panels were used for as-built characterization.

2.3 Metallography

Sections from the as-built and heat treated samples were used for metallographic examination. The sample sections were mounted in acrylic resin and rough polished using 240, 320, 400, 600, 800, and 1200 grit SiC abrasive paper (Figure 18).

Figure 18. JBK-75 and NASA-HR-1 samples mounted in acrylic resin.

Following rough polish, each sample was final polished using 6 μm, 3 μm, and 1 μm water-based diamond slurry. After final polish, samples were etched with either glyceregia, acetic glyceregia, or Kallings No. 2 etchant for roughly 5-10 minutes.

2.4 Tensile Testing

After all the samples were heat treated and machined into tensile specimens, they were tensile tested on an Instron 5584 (Figure 19). JBK-75 samples were tested with a crosshead displacement rate of 3.00 mm/min for the first 1.5% strain. An extensometer was used during the first 1.5% strain to accurately measure strain. Twenty-eight JBK-75 tensile specimens were tested. The NASA-HR-1 samples were also tested with a crosshead displacement rate of 3.00 mm/min. No extensometer was used due to the small nature of these samples. Twenty-four NASA-HR-1 tensile specimens were tested.

Figure 19. NASA-HR-1 sample in tensile test load frame.

3. Results

3.1 Characterization of As-Deposited Material

Metallographic examination and scanning electron microscopy were conducted to characterize the as-deposited material for both the JBK-75 and NASA-HR-1 samples. The goal of this characterization was to document how the microstructure of these alloys changes in response to the different heat treatments performed on each sample set. Figure 20a shows the microstructure of the as-built JBK-75 material normal to the build direction, and Figure 20b shows the microstructure transverse to the build direction. One important observation was the low degree of porosity observed throughout the microstructure – with these additive processing parameters, this as-built microstructure does not require a hot isostatic pressing (HIP) treatment to reduce porosity. As-built JBK-75 exhibited a columnar dendritic microstructure. This structure occurs due to the rapid heating and cooling rates of AM, which cause rapid solidification, causing a fine dendritic structure to form where dendrites grow in the direction of the melt pool solidification [8].

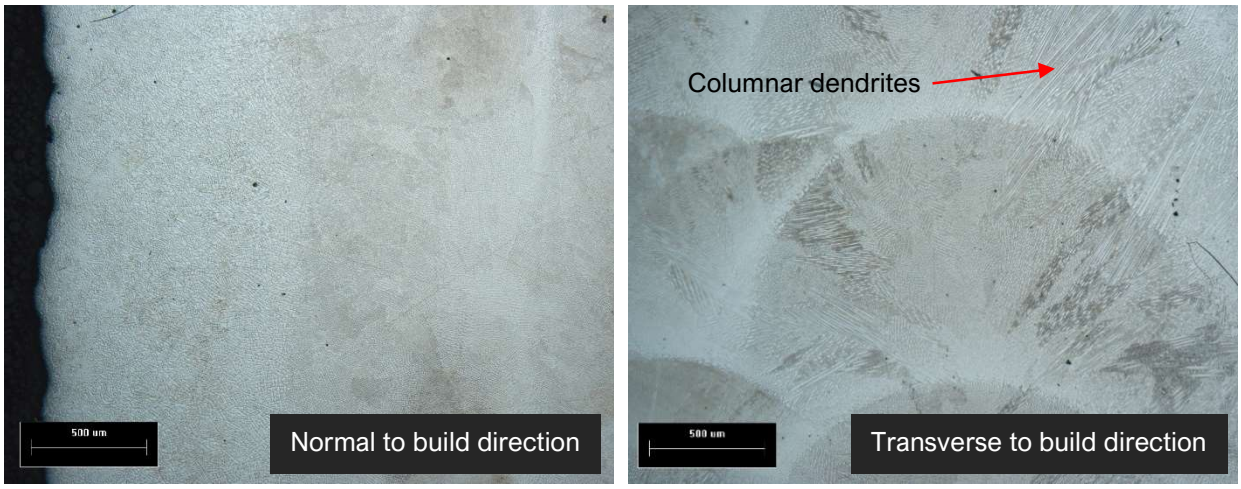

a. b.

Figure 20a. JBK-75 as-built microstructure normal to the build direction. Figure 20b. JBK-75 as-built microstructure transverse to the build direction. Etched with glyceregia, 50X magnification. Notice the predominance of columnar dendrites in the transverse direction.

Dendritic microstructures also exhibit microsegregation, where solute alloying elements are rejected into the liquid phase while the first solid dendrites form. These solute alloying elements are then segregated to the interdendritic regions of the microstructure. These compositional variations across the microstructure have been shown in the literature to cause an inhomogeneous response in age hardening, which is why the focus for this project is on the homogenization heat treatment step, which is meant to remove these differences in composition and to recrystallize the microstructure into an equiaxed structure. Figure 21a shows the JBK-75 as-built microstructure at 500X magnification, where the columnar dendrites and their secondary arms can be seen. Figure 21b shows this same microstructure under a scanning electron microscope, where the secondary dendrite arm spacing was measured to be roughly 0.08 mils, or 2 μm.

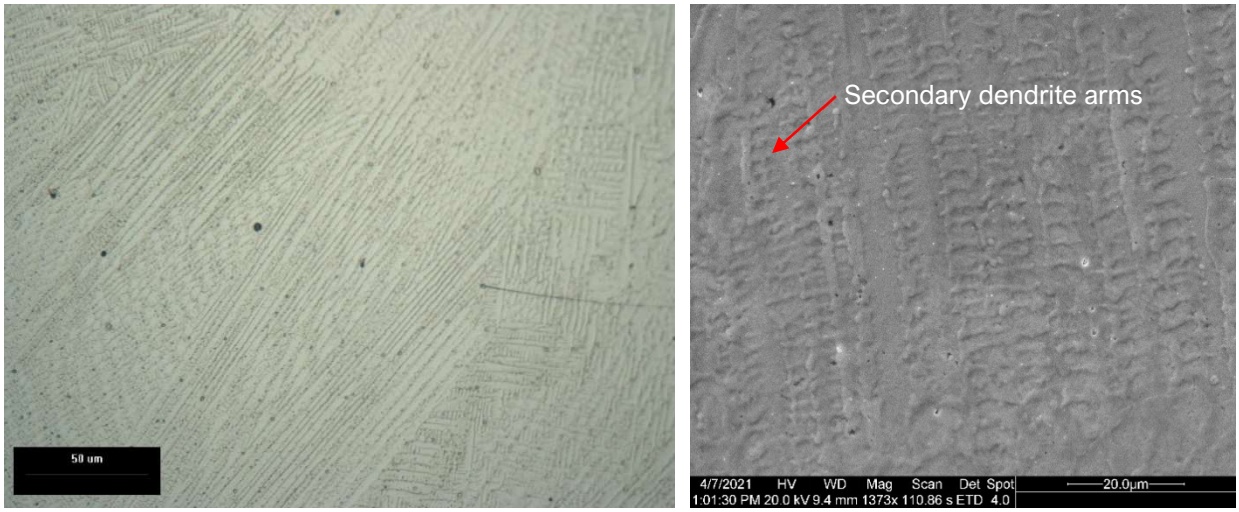

a. b.

Figure 21a. As-built JBK-75 microstructure showing columnar dendrites, 500X magnification. Figure 21b. SEM image of as-buiilt microstructure at roughly 1400X magnification. Etched with glyceregia.

As for the as-built NASA-HR-1 material, several key differences in the microstructure were observed. Figure 22a shows the microstructure of Box 1 HR-1 in the as-built condition, and Figure 22b shows the microstructure of Box 2 in the as-built condition, both at 50X magnification. Notice the higher porosity and surface roughness for Box 2 HR-1. As shown in the following sections, both the porosity and surface finish had a noticeable effect on the ductility of these samples, especially since the samples were thin.

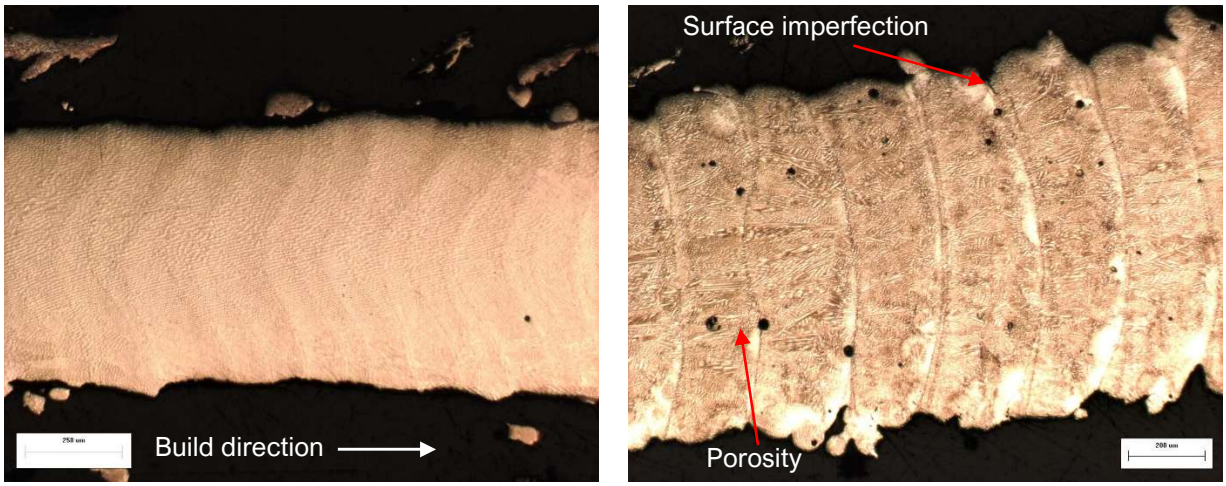

a. b.

Figure 22a. Box 1 as-built HR-1 microstructure. Figure 22b. Box 2 as-built HR-1 microstructure. 50X magnification, etched with glyceregia.

Figure 23a and 23b shows the microstructure of both Box 1 and Box 2 HR-1 at a higher magnification, showing a similar columnar dendritic microstructure as the JBK-75 as-built samples. Boxes 1 and 2 had similar secondary dendrite arm spacings, meaning that the micro-segregation should be to a similar degree for both sample boxes.

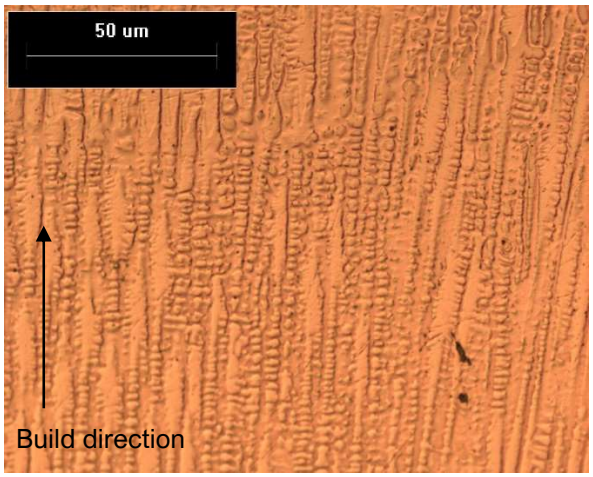

a.

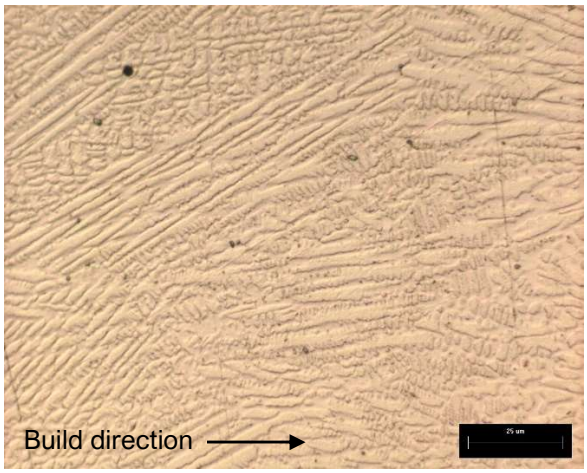

b.

Figure 23a. Box 1 HR-1 microstructure. Figure 23b. Box 2 HR-1 microstructure. 500X magnification, etched with glyceregia.

3.2 Tensile Testing Results for Heat Treated JBK-75

For the JBK-75 sample set, four tensile specimens were tested per heat treatment category. Figure 24 shows a summary of yield strength results for each of the heat treatment categories. The yield strength of wrought, solution treated, and aged JBK-75 is also shown on the chart. The samples that were not homogenized, only solution treated and aged showed the highest yield strength from all heat treatments tested. Among the homogenized sample lots, there was little variation in yield strength, and homogenization time and temperature did not appear to have a significant effect on yield strength beyond 2 hours. All samples met or surpassed the typical yield strength of wrought JBK-75 in the solution treated and aged condition.

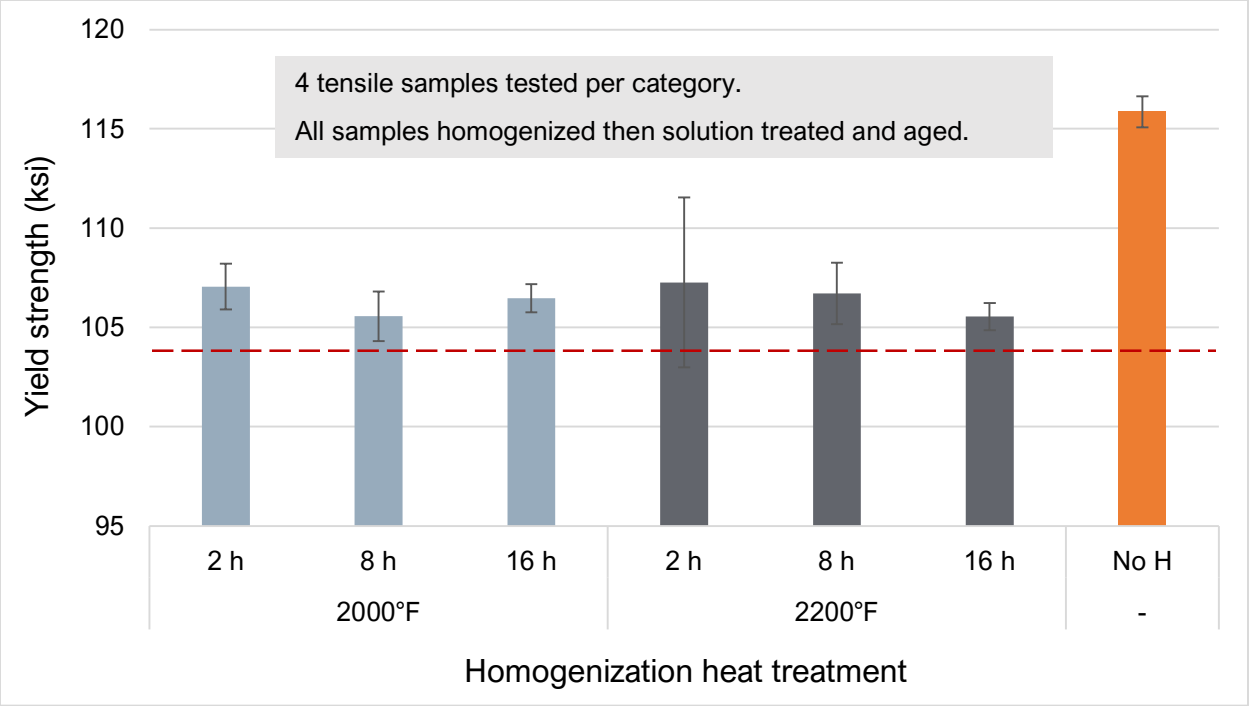

Figure 24. Yield strength data summary for heat treated JBK-75. Error bars denote one standard deviation.

Figure 25 shows a plot of yield strength versus homogenization time, which shows that homogenization time and temperature did not have a significant effect on yield strength.

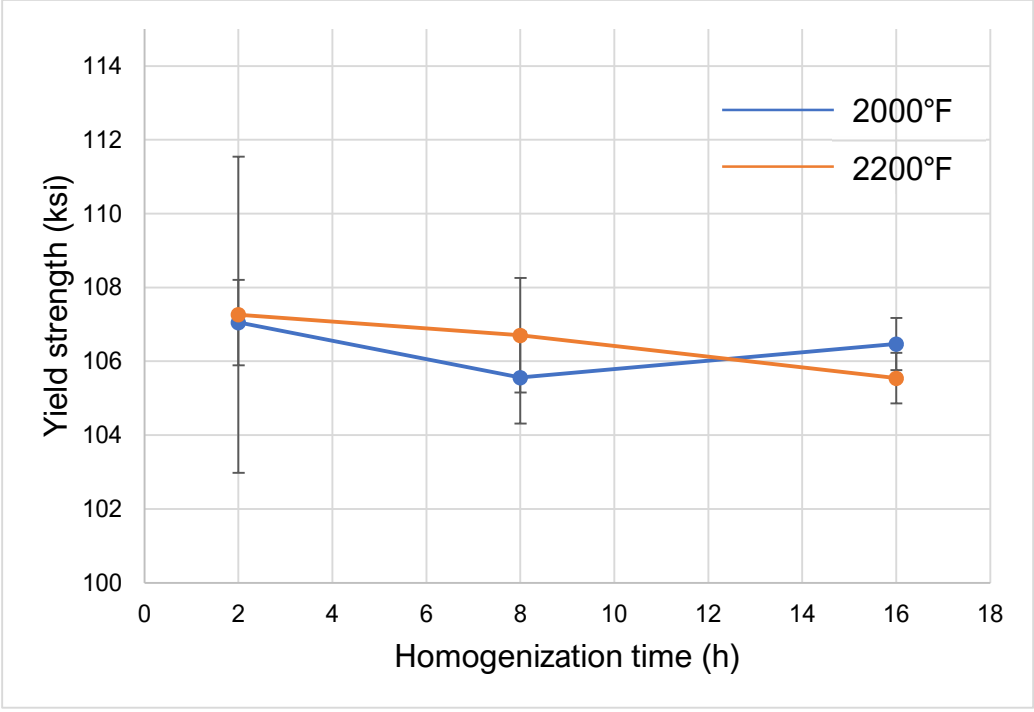

Figure 25. Plot showing the lack of effect of homogenization time and temperature on yield strength in the time and temperature ranges evaluated.

Figure 26 shows a similar summary as Figure 24 for tensile strengths for each heat treatment category. Interestingly, the non-homogenized samples did not have the highest ultimate tensile strength, which is different from the yield strength data, where the non-homogenized samples exhibited roughly a 10 ksi higher yield strength than most homogenized samples. Additionally, no samples reached the typical tensile strength for wrought, solution treated and aged JBK-75.

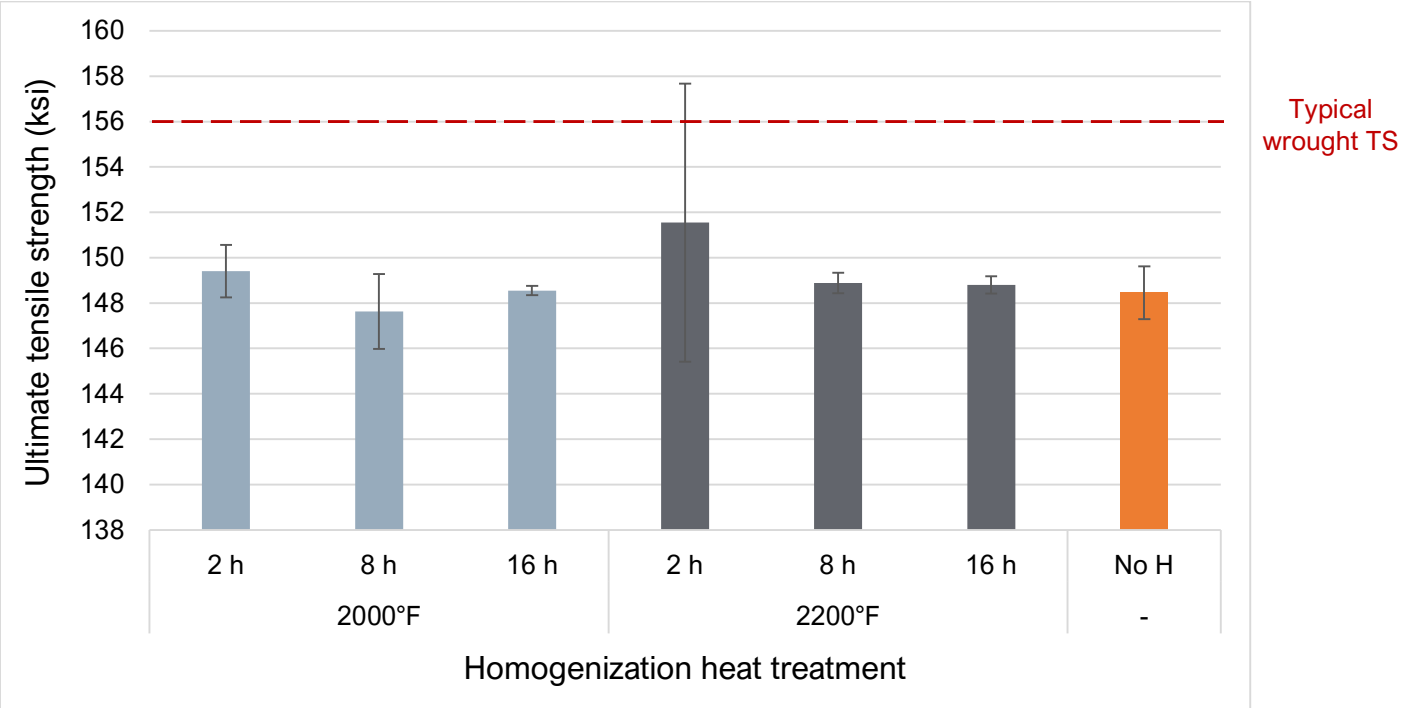

Figure 26. Tensile strength results summary for heat treated JBK-75. Notice that the non-homogenized samples were not the strongest, unlike what the yield strength data showed.

Figure 27 shows the ductility results for all samples. It is important to note that several sample groups have a large spread in elongation values. Figure 28 illustrates where this large spread in elongation originates. A group of samples exhibited much lower ductility than the typical 25-30% elongation exhibited by most samples. These samples are highlighted in red on the stress-strain plot. There was no clear trend as to which heat treatments tended to have low ductility samples.

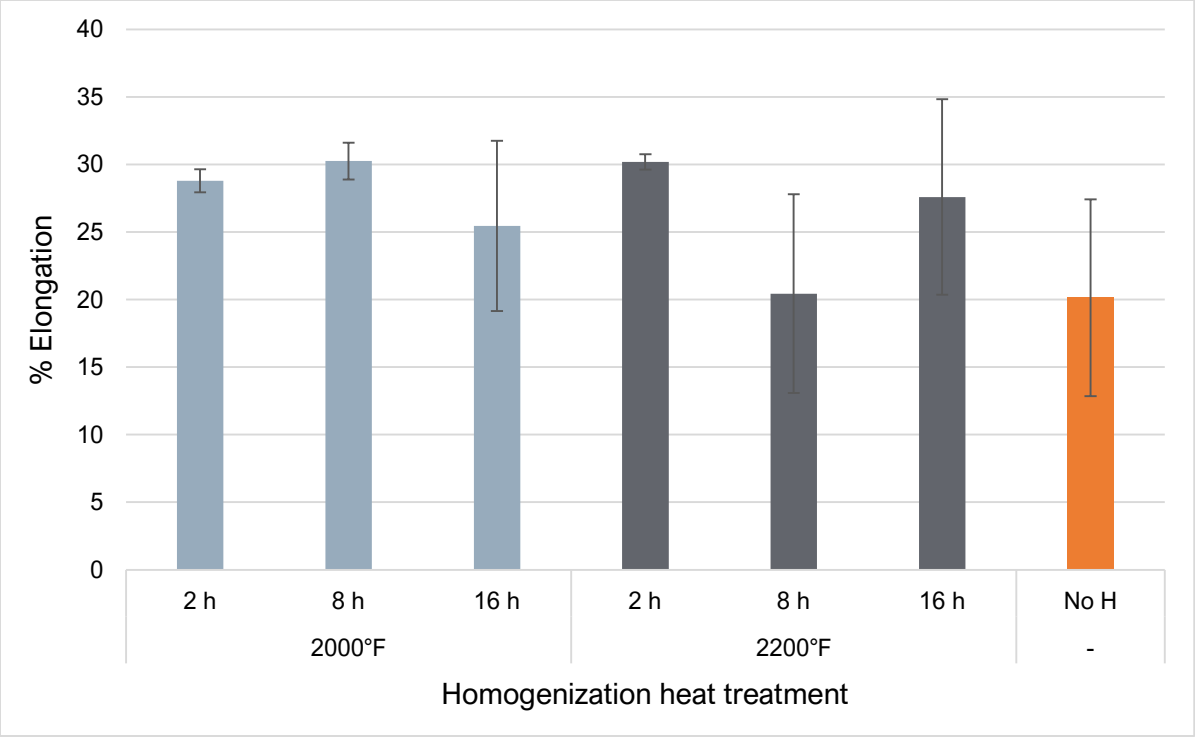

Figure 27. JBK-75 elongation results summary. Notice that several sample sets have more extreme variety due to some samples exhibiting half of their typical ductility.

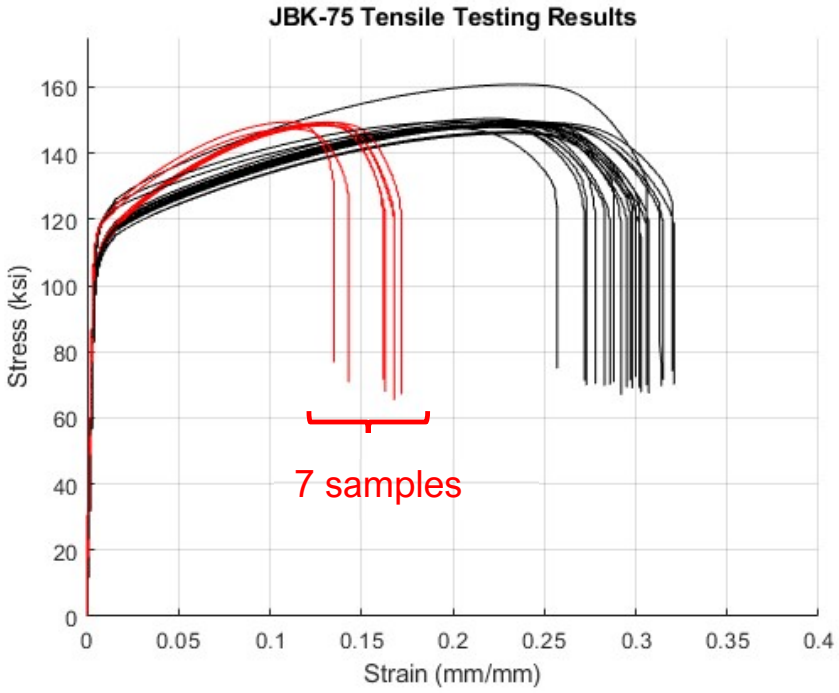

Figure 28. JBK-75 tensile testing stress-strain curves. Low ductility samples are highlighted in red.

Table IV shows which heat treatment categories had samples that exhibited how ductility. There was no clear trend as to which samples exhibited normal ductility and which samples showed low ductility.

Table IV. Low Ductility Samples by Heat Treatment Category

Homogenization heat treatment	Samples with low ductility (out of 4 tested)
2000°F, 2 h	None
2000°F, 8 h	None
2000°F, 16 h	1
2200°F, 2 h	None
2200°F, 8 h	3
2200°F, 16 h	1
No homogenization	2

To investigate the cause of these differences in yield strength and ductility, metallographic examination was performed on all samples.

3.3 Characterization of Heat Treated JBK-75

Samples from each heat treatment category were mounted and examined metallographically for any microstructural differences that could be causing these differences in mechanical properties for certain samples. Figure 29 shows the microstructure of a homogenized, solution treated, and aged JBK-75 sample. This sample was homogenized at 2200°F for 16 hours, followed by the standard solution treat and age. Notice that the material has recrystallized into an equiaxed structure, and that any indication of the dendritic structure is gone, meaning that the material has fully homogenized. All homogenized samples both fully recrystallized and fully homogenized. However, all homogenized samples exhibited a coarse grain size and a high number of annealing twins, which is evidence that significant grain growth occurred. This means that the homogenization heat treatments were too long, and a shorter time can be used while still achieving an equiaxed, recrystallized, and homogeneous microstructure.

Figure 29. Heat treated JBK-75 microstructure - homogenized at 2200°F for 16 hours. 100X magnification. Etched with Kallings No. 2. Note that all homogenized samples exhibited a similar coarse-grained, equiaxed microstructure.

On the other hand, the non-homogenized samples exhibited a different morphology. Figure 30 shows the microstructure of a non-homogenized JBK-75 sample that has only been solution treated and aged. These samples recrystallized as evidenced by grain boundaries that were not present prior to solution treating and aging, meaning that heat treatment at 1800°F for 1 hour (standard solution heat treatment) is sufficient for recrystallization. However, these samples did not fully homogenize – the prior dendritic structure is still visible upon etching, meaning that some degree of microsegregation is still present in the microstructure. The team expected that the lack of full homogenization would negatively affect the age hardening response and decrease strength, but these samples exhibited the highest yield strength.

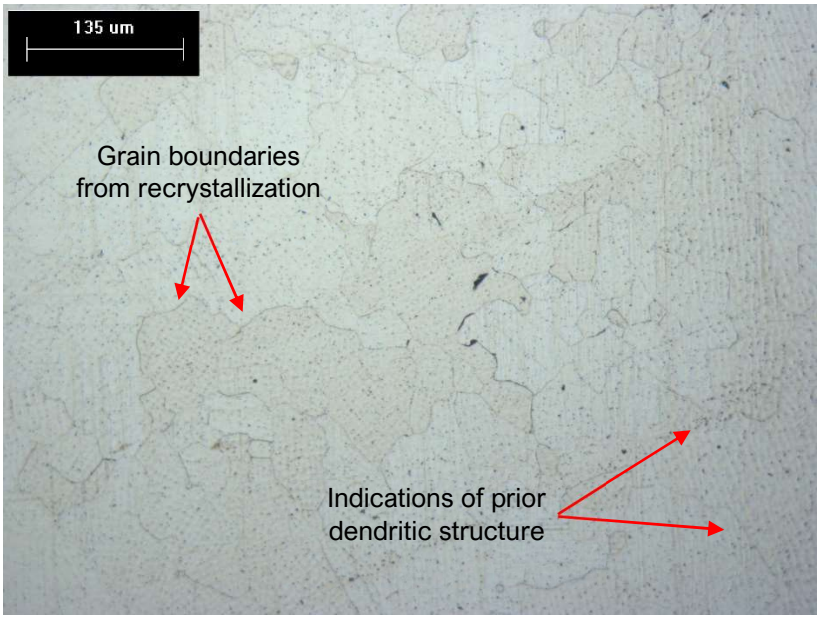

Figure 30. Non-homogenized, solution treated and aged JBK-75 microstructure. 200X magnification. Etched with glyceregia.

One potential difference in microstructure that could have caused this increase in yield strength for the non-homogenized samples is grain size. Figure 31 shows a plot of grain size versus yield strength for all JBK-75 samples. Grain size was measured according to ASTM E1382. Notice that the non-homogenized samples had the finest grain size at roughly ASTM 3-4, while the homogenized samples exhibited a coarser grain size of roughly ASTM 6-7.

Figure 31. ASTM grain size versus yield strength for heat treated JBK-75. The non-homogenized samples experienced low grain growth and showed a higher strength. Grain size measured using ASTM E1382.

As mentioned before, several samples exhibited low ductility. Figure 32a shows the microstructure of a homogenized, solution treated, and aged JBK-75 sample at 500X magnification. Secondary phase precipitation was observed at the grain boundaries. Figure 32b shows the region of the microstructure enclosed by the red box at 1000X magnification. Indications of a second phase that precipitated along the grain boundaries were observed, based on the increased thickness of some regions of the grain boundaries when etched. Grain boundaries are a common place for both carbides and η to nucleate, but without energy dispersive X-ray analysis (EDS), the team was unable to confirm the presence of these phases. However, the TTP diagram for JBK-75 shows that the aging heat treatment of 1375°F for 16 hours passes well into the precipitation region for MC carbides and at around 14-15 hours passes into the start of η precipitation, meaning the presence of both phases is possible. The literature also shows that $M_{23}C_6$ and M_6C carbides can also form films along the grain boundaries like MC carbides [10]. The presence of either grain boundary carbides or η is known to reduce ductility – this remains a possible cause for some samples having low ductility but also requires further investigation [10].

a. b.

Figure 32a. Homogenized, solution treated, and aged JBK-75 microstructure at 500X magnification. Figure 32b. Region of the microstructure highlighted in red in Figure 32a, at 1000X magnification.

Precipitation of a secondary phase along the grain boundaries was also observed for the non-homogenized samples. Figure 33 shows the microstructure of a non-homogenized, solution treated, and aged JBK-75 sample at 1000X magnification. Notice the cellular structures along the grain boundaries indicated by the red arrows. This cellular morphology is consistent with η phase, which forms due to locally enriched titanium content or prolonged high temperature exposure. Because these samples were not homogenized, the formation of η in this case can likely be attributed to local titanium enrichment, which is an artifact of the microsegregation produced during the additive manufacturing process. As discussed earlier, this microsegregation was not fully eliminated by only the solution treatment and may have altered the alloy's precipitation kinetics, favoring η precipitation. Ultimately, further microstructural analysis using SEM and EDS characterization techniques would be necessary to study these phases in finer detail, given their scale in the microstructure.

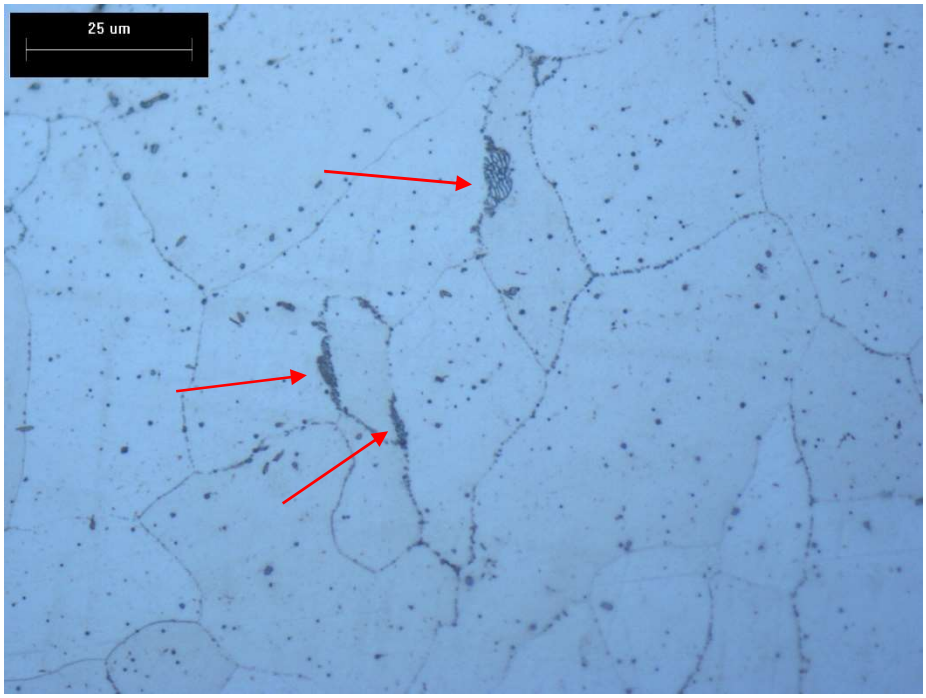

Figure 33. Microstructure of non-homogenized JBK-75 sample at 1000X magnification. Regions with heavy η precipitation are indicated by red arrows. The cellular morphology indicates η rather than carbides.

Overall, the team found that full homogenization and recrystallization can be achieved at the lowest tested homogenization temperature and time of 2000°F for 2 hours. It was also found that recrystallization could occur during the lower solution treatment temperature of 1800°F, but 1 hour at this temperature was not sufficient to homogenize the material. The optimum homogenization treatment would lie somewhere between these two times and temperatures, and a further study is recommended to determine that optimal heat treatment.

3.4 Tensile Testing Results for Heat Treated NASA-HR-1

The NASA-HR-1 tensile test results showed that there are factors in the initial processing, surface finish, and heat treatment that all negatively affected the alloy's strength and ductility. Figure 34 shows a chart of yield strengths for each different homogenization heat treatment for the NASA-HR-1 samples. Unlike the JBK-75 samples, the non-homogenized samples did not exhibit a higher yield strength. Furthermore, all samples fell far below where the expected yield strength would be for this alloy – the typical yield strength of wrought HR-1 in the solution treated and aged condition is 136 ksi [8]. While it is expected that the strength of material produced by DED will be lower than that of wrought material, other factors are causing these low yield strengths.

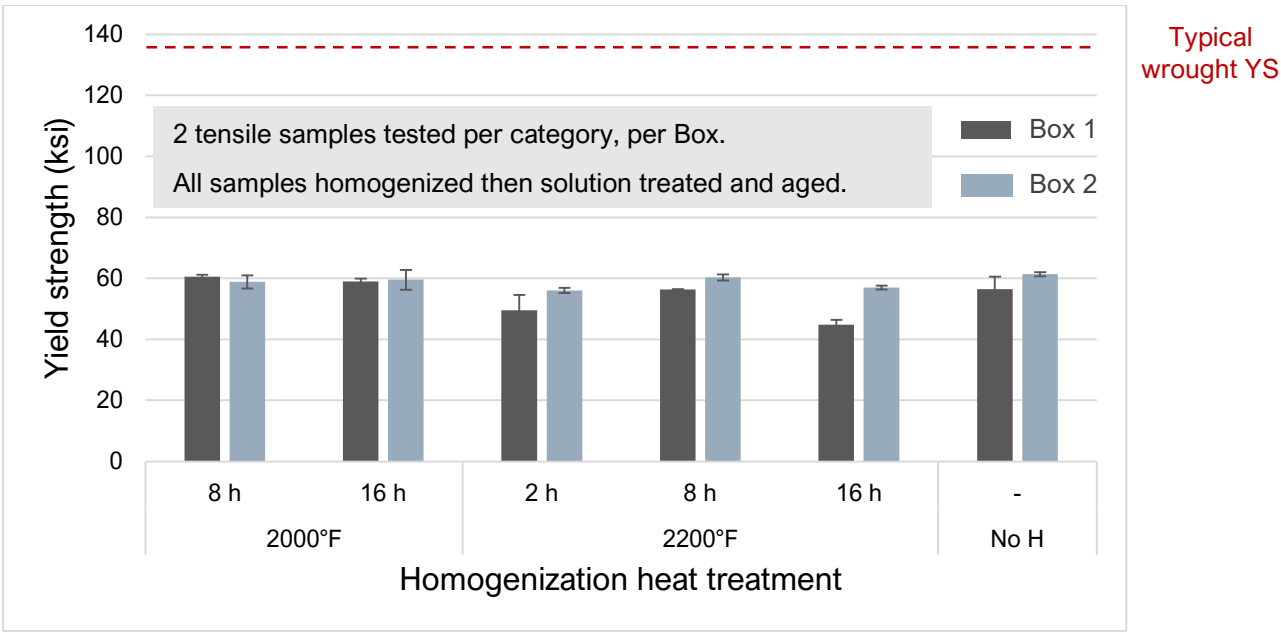

Figure 34. NASA-HR-1 yield strength summary. Box 1 HR-1 is denoted by the darker bars, and Box 2 HR-1 is denoted by the light bars. The typical wrought, heat treated yield strength is shown on the chart as well.

Figure 35 shows a summary of ultimate tensile strengths for the NASA-HR-1 samples. Once again, these samples fell far below the wrought strength. The Box 2 samples showed a slightly higher yield and tensile strength than the Box 1 samples. In terms of differences in mechanical properties due to varying heat treatments, no significant differences or trends were observed. Yield and tensile strength appeared to be independent of homogenization time and temperature in the ranges that were studied.

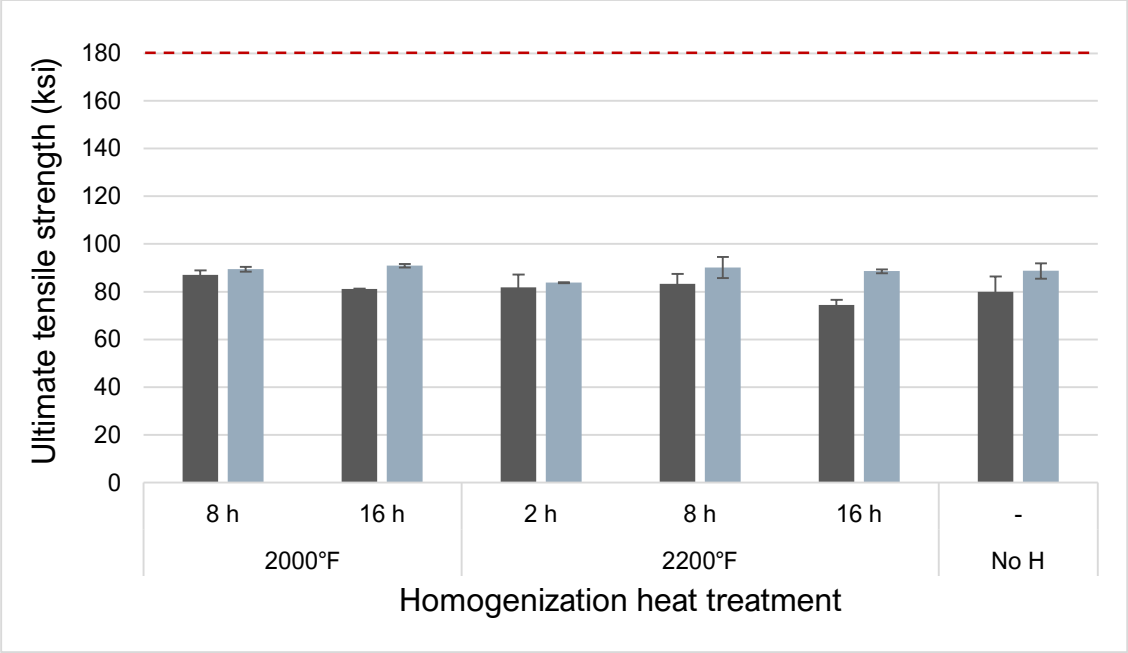

Figure 35. NASA-HR-1 tensile strengths summary. Notice that all samples fell well below the typical wrought strength for this alloy. Additionally, no significant trends were observed based on varying homogenization treatments.

In terms of ductility for these samples, the team did observe significant differences between Box 1 and Box 2. Figure 36 shows a summary of percent elongation data from the NASA-HR-1 samples. Across almost all homogenization heat treatments, the Box 1 samples exhibited greater ductility than the Box 2 samples. One possible cause for this low ductility was shown in the initial characterization of these samples. Box 2 HR-1 samples showed a high degree of porosity in the as-built condition, as well as a high surface roughness with lots of sharp imperfections that could have a notch effect during a tensile test, reducing the ductility. The team investigated this further through metallography on all homogenized, solution treated, and aged samples. Across samples from the same box, ductility was also highly inconsistent and variable, and this attribute is only exacerbated due to the small sample size of 2 samples per homogenization time/temperature combination.

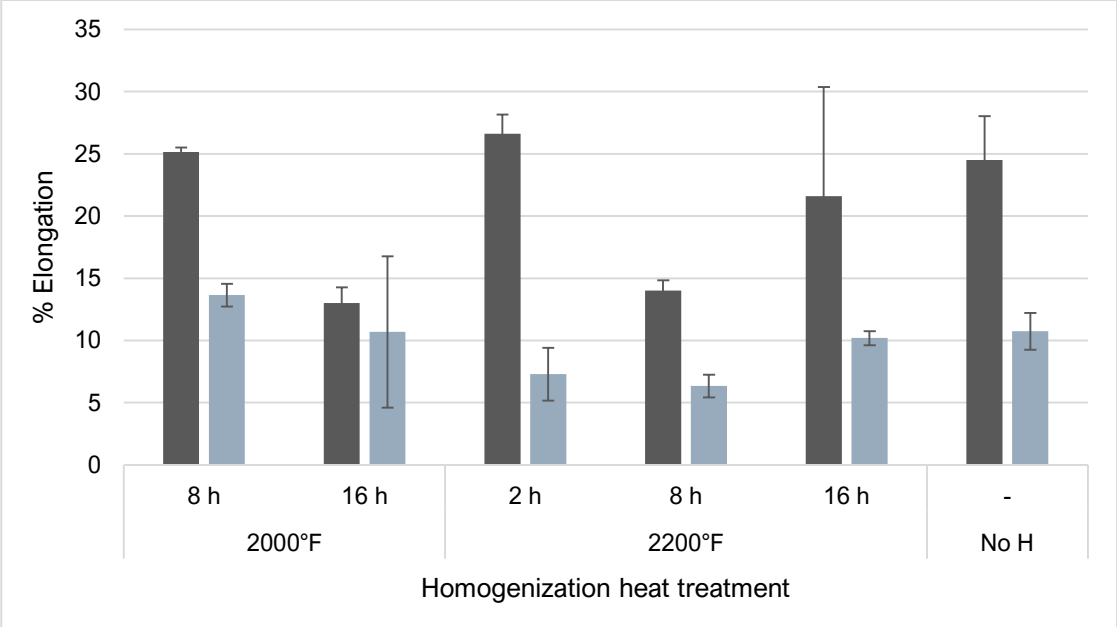

Figure 36. NASA-HR-1 summary of ductility data from tensile testing. Notice that the Box 2 samples generally showed much lower ductility than Box 1 samples.

3.5 Characterization of Heat-Treated NASA-HR-1

To better understand the significant differences in mechanical properties between the JBK-75 and HR-1 samples, all HR-1 samples were examined metallographically. Figure 37a shows the microstructure of a homogenized sample from Box 1, and Figure 37b shows a homogenized sample from Box 2. Both images were taken at 100X magnification. Once again, the difference in both surface finish and porosity can be seen where Box 2 has a high surface roughness and high porosity compared to Box 1. Additionally, the team observed a large difference in the recrystallization behavior of the material – Box 1 showed extremely large grain sizes on the order of 100-200 μm in width, and several millimeters long in the build direction, while Box 2 showed an equiaxed grain structure with grain sizes in the range of ASTM 4-5. This difference in grain size could be a possible reason for the slightly higher strength of Box 2 HR-1, as a higher density of grain boundaries presents more barriers to dislocation motion, as well as more regions for carbides to nucleate and strengthen the material further.

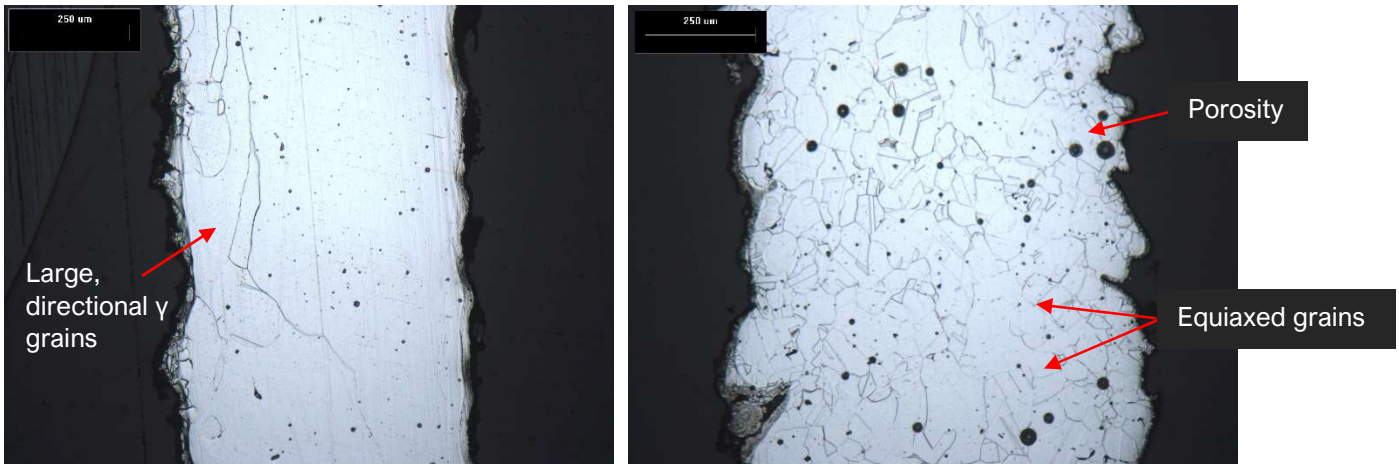

a. b.

Figure 37a. Box 1 microstructure, 100X magnification. Figure 37b. Box 2 microstructure, 100X magnification. Etched with Kallings No. 2 reagent. Both samples were homogenized at 2000°F for 16 hours, then solution treated and aged.

Non-homogenized NASA-HR-1 samples did not exhibit a significantly different structure than the homogenized samples as shown by Figure 38a and b, but this is likely because the stress relief heat treatment also permitted recrystallization and homogenization of the structure at 1950°F. The combination of stress relief, homogenization, and solution treatment is unnecessary, as the alloy can likely homogenize and recrystallize in 2-3 hours at 1950-2000°F, permitting a single heat treatment in that temperature range, followed by a quench to room temperature before the subsequent age hardening heat treatment.

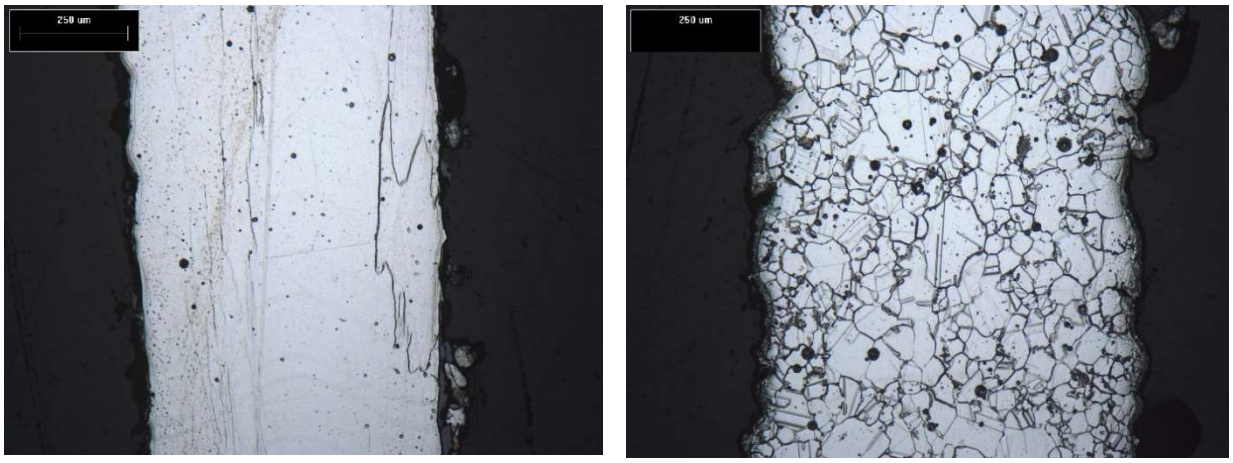

a. b.

Figure 38a. Box 1 non-homogenized HR-1 microstructure. Figure 38b. Box 2 non-homogenized HR-1 microstructure. 100X magnification. Etched with Kallings No. 2 reagent.

The team also measured grain size for all Box 2 HR-1 samples but found only a weak correlation between yield strength and grain size, but this is likely because the homogenization heat treatments were too long, and these treatment times were at the tail end of the recrystallization

and grain growth process, which is why there is little variation in grain size among the homogenized samples. Figure 39 shows these results. One consistent result with JBK-75 is that the non-homogenized sample showed the highest yield strength and exhibited the smallest grain size.

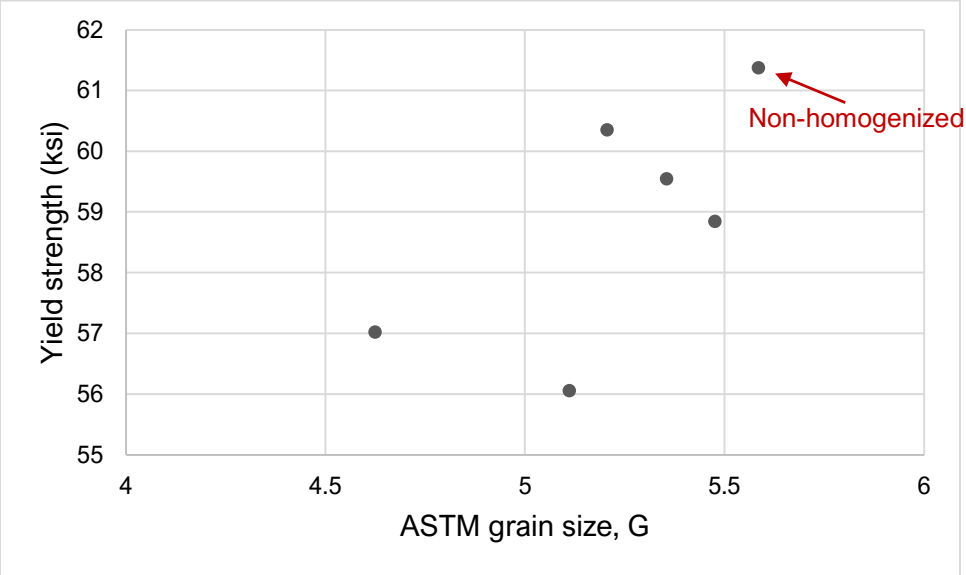

Figure 39. ASTM grain size versus yield strength for Box 2 HR-1 heat treated samples.

4. Discussion

4.1 Discussion of JBK-75 Results

In terms of the overall design of experiment, the range of homogenization times was too long for the level of segregation observed in the microstructure. The reasoning for this comes from observing the microstructure of JBK-75 at the lowest homogenization time and temperature of 2000°F for 2 hours – significant grain growth occurred past recrystallization, meaning that shorter times and/or lower temperatures can be used for this heat treatment. Past 2 hours, there was no evidence of significant change in grain size or mechanical properties, meaning that there would be no reason to homogenize a part for longer than 2 hours at 2000°F, which is a positive finding from a manufacturing cost perspective.

Repeating this study with shorter homogenization times, lower temperatures, and no solution heat treatment would be necessary to determine the minimum heat treatment times necessary to achieve optimum properties. It became clear based on the data that the largest microstructural changes occur in the first 30 minutes to 2 hours in the temperature range of 1800-2000°F, whereas microstructural changes past that time are negligible. Additionally, incorporating EDS analysis of the as-built dendritic structure and diffusion modeling into selecting homogenization times and temperatures could allow for a better estimation of the optimum homogenization heat treatment prior to experimental studies. However, even with longer than necessary homogenization times, a high strength level of roughly 100 ksi or greater was still reached for most samples.

4.2 Discussion of NASA-HR-1 Results

NASA-HR-1 had similar results to JBK-75 in terms of homogenization times – the range of homogenization times was shifted towards being too long, and microstructural changes would best be studied in the range of 30 minutes to 2 hours at 1950-2000°F. An additional significant influence on the results of the NASA-HR-1 study was the DED processing parameters of the as-built material. Porosity, surface roughness, and differences in initial microstructure between Box 1 and Box 2 all had effects on the results for this alloy. Porosity and surface roughness appeared to play a significant role in limiting the ductility of the Box 2 samples, while the as-built microstructure for Box 1 appeared to affect the recrystallization behavior where long, directional grains formed, rather than equiaxed grains. The cause of this behavior is still unknown and an item for future work. The team did not have time to investigate this further, but some unknown factor was significantly limiting the strength of the NASA-HR-1 samples. One potential characterization method to further investigate this low strength would be SEM imaging of the microstructure at high magnification to examine the precipitation of γ', since these precipitates are mainly responsible for the strength of this alloy. Ultimately, further investigation of the results from this study are mainly an item for future work, since there were many different variables such as surface finish, porosity, secondary phase precipitation, and differences in recrystallization.

5. Conclusions

5.1 JBK-75 Conclusions

1. Recrystallization and full homogenization can be achieved with the lowest selected homogenization temperature and time (2000°F for 2 hours). Past 2 hours, homogenization time had no effect on yield strength.

2. The strength of wrought JBK-75 was reached with all DED JBK-75.

3. The non-homogenized samples exhibited the highest yield strength. This is potentially caused by the finer grains found in the non-homogenized samples.

4. There is potential for large losses in ductility. One potential cause is the precipitation of ductility limiting phases in the grain boundaries, but this remains an item for future work.

5.2 NASA-HR-1 Conclusions

1. The surface quality and porosity due to DED parameters lead to a large difference in ductility between the two NASA-HR-1 samples. Box 2 HR-1 had a significantly higher degree of porosity and high surface roughness as evidenced by metallography.

2. The strength of the DED NASA-HR-1 did not meet the typical strength of wrought NASA-HR-1.

3. The DED processing parameters and as-built microstructure influenced the recrystallization behavior, causing differences in the microstructure between Box 1 and Box 2 HR-1.

4. All the Box 2 HR-1 samples exhibited full recrystallization into an equiaxed structure, including the sample that was not homogenized.

6. Recommendations

6.1 JBK-75 Recommendations

1. Homogenization heat treatment can be incorporated into the same step as the solution heat treatment. There was evidence in the non-homogenized samples of recrystallization. Therefore, a combined homogenization-solution treatment step would save in overall cost while still allowing for full homogenization and recrystallization of the microstructure. This homogenization-solution treatment step does not need to be longer than 2 hours and could most likely be shorter.

2. Study the occurrence of low ductility samples and what aspects of the microstructure and heat treatment influence this behavior.

6.2 NASA-HR-1 Recommendations

1. Further DED process parameter development is recommended to decrease porosity and improve surface finish.

2. Study the effect of DED process parameters and as-built microstructure on recrystallization behavior.

3. Integrate homogenization heat treatment step into the solution treat step. The homogenization times could be significantly shorter than the shortest time tested in this study (2 hours).

4. Investigate the cause of low strength in NASA-HR-1 samples.

7. References

[1] "RS-25 Engine." [Online]. Available: https://www.rocket.com/space/liquid-engines/rs-25-engine. [Accessed: 02-Feb-2021].

[2] P.R Gradl, "Advancement of Metal Additive Manufacturing Technique and Materials for Rocket Propulsion Applications". DOI: 10.13140/RG.2.2.23927.65444

[3] B. Evans, "NASA Orders 18 More RS-25 Engines for SLS Moon Rocket, at $1.79 Billion," *AmericaSpace*, 04-May-2020. [Online]. Available: https://www.americaspace.com/2020/05/02/nasa-orders-18-more-rs-25-engines-for-sls-moon-rocket-at-1-79-billion/. [Accessed: 02-Feb-2021].

[4] J.-H. Kwon, J. Periaux, and P. Fox, *Parallel Computational Fluid Dynamics*. Amsterdam: Elsevier Science, 2007.

[5] "RS-25," *Wikipedia*, 31-Jan-2021. [Online]. Available: https://en.wikipedia.org/wiki/RS-25. [Accessed: 02-Feb-2021].

[6] P. R. Gradl and C. S. Protz, "Technology advancements for channel wall nozzle manufacturing in liquid rocket engines," *Acta Astronaut.*, vol. 174, pp. 148–158, Sep. 2020, doi: 10.1016/j.actaastro.2020.04.067.

[7] J. A. Fint *et al.*, "(12) United States Patent," 2009.

[8] C. Katsarelis *et al.*, "Additive Manufacturing of NASA HR-1 Material for Liquid Rocket Engine Component Applications." [Online]. Available: https://ntrs.nasa.gov/search.jsp?R=20200001007.

[9] B. Pollard, "Selection of Wrought Precipitation-Hardening Stainless Steels," *ASM Handbook*, vol. 6, pp. 482–494, 1993.

[10] L. Li, "Heat Treating of Precipitation-Hardenable Stainless Steels and Iron-Base Superalloys," *ASM Handb.*, vol. 4, pp. 397–417, 2018, doi: 10.31399/asm.hb.v04d.a0005961.

[11] P. Chen and M. Mitchell, "NASA-HR-1 overview," 2005.

[12] N. S. Stoloff, "Wrought and P/M Superalloys," *ASM Handbook*, vol. 1, pp. 950–980, 2018, doi: 10.31399/asm.hb.v01.a0001049.

[13] T. J. Headley, M. M. Karnowsky, and W. R. Sorenson, "Effect of composition and high energy rate forging on the onset of precipitation in an iron-base superalloy," *Metall. Trans. A*, vol. 13, no. 3, pp. 345–353, 1982, doi: 10.1007/BF02643343.

[14] G. F. Vander Voort and G. M. Lucas, "Metallography and Microstructures of Stainless Steels and Maraging Steels[1]," *ASM Handbook*, vol. 9, no. c, pp. 670–700, 2018, doi: 10.31399/asm.hb.v09.a0003767.

[15] ASTM International. (2016). Standard Guide for Directed Energy Deposition of Metals. *ASTM Standard*, 1–22. https://doi.org/10.1520/F3187

[16] Valdivieso, C. (2019). The Complete Guide to Directed Energy Deposition (DED) in 3DPrinting. In *3D natives*. https://www.3dnatives.com/en/directed-energy-deposition-ded-3d-printing-guide-100920194/#!

[17] Bauer, T., Dawson, K., & Spierings, A. (2015). *Microstructure and mechanical characterisation of SLM processed Haynes® 230®*. 813–822.

[18] Bourell, D. L., & Wohlers, T. (2020). Introduction to Additive Manufacturing. *Additive Manufacturing Processes*, *24*, 3–10. https://doi.org/10.31399/asm.hb.v24.a0006555

[19] ASTM International. (2021). Standard Test Methods for Tension Testing of Metallic Materials. *ASTM Standard,* DOI: 10.1520/E0008_E0008M-21